Journal of MATERIALS RESEARCH

Article
DOI:10.1557/s43578-023-01077-8

Effect of lanthanum doping on structural, optical, and photocatalytic properties of YVO_4

Erkul Karacaoglu[1,a], Ozlem Altintas Yildirim[2,3], Teoman Ozturk[4,5], Mert Gul[6]

[1] Metallurgy and Materials Engineering, Karamanoglu Mehmetbey University, Karaman, Türkiye
[2] Metallurgical and Materials Engineering, Faculty of Engineering and Natural Sciences, Konya Technical University, Konya, Türkiye
[3] Nanotechnology and Advanced Materials Development, Application and Research Center, Konya Technical University, Konya, Türkiye
[4] Department of Physics, Faculty of Science, Selcuk University, Konya, Türkiye
[5] Advanced Technology Research and Application Center, Selcuk University, Konya, Türkiye
[6] Materials Science and Engineering, Eskisehir Technical University, Eskisehir, Türkiye
[a] Address all correspondence to this author. e-mail: ekaracaoglu@kmu.edu.tr

Received: 17 January 2023; accepted: 2 June 2023; published online: 20 June 2023

In this study, we report the solid-state reaction synthesis of yttrium vanadate (YVO_4)-based undoped and lanthanum (La)-doped powders. The photocatalytic performances, structural, morphological, and optical analyzes are presented. The X-ray diffraction analysis of samples indicates the crystalline tetragonal type crystal structure of YVO_4 and no other lanthanum related impurity and/or secondary phases were detected. Photoluminescence analysis of samples show combined white light emission peaks that appeared at 478, 571 and 613 nm. To examine the photocatalytic activities, the degradation of methylene blue (MB) dye was monitored in the presence of these photocatalysts under the ultraviolet light irradiation. Pseudo-first-order reaction rate constant (k) of YVO_4:La^{3+} (0.00846 min^{-1}) is determined 66% greater than undoped one (0.00287 min^{-1}). These results are compatible with the absorption spectra, as the energy band gap of the undoped photocatalyst was 3.8 eV while that of the doped one decreased to 3.54 eV.

Introduction

Water pollution due to industrialization and increasing need for fresh water with rapid population growth have become a major environmental problem worldwide. Moreover, another harsh truth is that only 2.5% of the total water volume in the world is fresh water [1]. Furthermore, the covid 19 pandemic has made clear that water purification, hygiene and wastewater treatment are not only beneficial to the environment but also to human health. For the wastewater treatment, many technologies were reported such as flotation, precipitation, membrane filtration, ozonation, coagulation-flocculation and photocatalysis [2–4]. Among these techniques, photocatalysis is getting more and more attention due to its low cost, environmental friendliness, and no secondary waste generation. Semiconductor photocatalysts have been used extensively as remediation materials for the degradation of environmental pollutions in wastewater such as organic pollutants, synthetic dyes, pesticides, herbicides, and antibiotics [5–10]. Since Fujishima and Honda demonstrated the splitting of water on a TiO_2 electrode [11], a tremendous effort has been endeavored to better understand the photocatalytic reaction mechanisms and to develop novel heterogeneous semiconductor photocatalysts. While these developed photocatalysts can be a binary structure such as TiO_2, ZnO, CdS, ZnS, Fe_2O_3, etc. [12–16], there is a remarkable increase in the use of novel ternary semiconductors such as Bi_2WO_6, Zn_2SnO_4, $La_2Ti_2O_7$, Bi_2MoO_6, BiOCl, etc. [17–21]. Most photocatalysts suffer from rapid recombination of photo-generated charge carriers, inefficient surface states and insufficient absorption of light. To overcome these disadvantages, many processes such as doping, composite engineering and surface modification have been tried [22–25]. As an alternative, oxygen vacancies on the surface of semiconductor photocatalysts can be considered as desired defect engineering [26]. Thus, it makes sense to deal with semiconductor photocatalysts that have both good crystallinity and oxygen vacancies.

Yttrium vanadate (YVO_4) can be taken as a model semiconductor photocatalyst due to its crystal structure and the ability to introduce oxygen vacancies through heat [27]. YVO_4 has a wide

band gap energy (3.8 eV) and can be excited by ultraviolet (UV) light [28]. Although the use of only UV irradiation is considered a disadvantage in terms of photocatalysis, the wide band gap of YVO_4 allows the excited electrons and holes to exhibit a strong redox capability [29]. Besides, YVO_4 nanostructures exhibit high thermal, mechanical, and chemical stability and have a strong birefringence which is well convenient for many optical applications [30, 31].

In one of the first studies on the photocatalytic of YVO_4, Xu et al. synthesized YVO_4 nanopowders via microwave irradiation and investigated their photocatalytic properties via decolorization of methyl orange [32]. Liu et al. prepared YVO_4 nanoparticles via molten salt method at a low temperature and their photocatalytic activity was investigated by the degradation of rhodamine B (RhB) [33]. Yang et al. produced YVO_4 nanoparticles at room temperature by a direct precipitation method which provide to control the crystallinity and concentration of oxygen vacancies, so provide to enhance in the photocatalytic efficiency of YVO_4 nanoparticles [27]. Sized-controlled YVO_4 nanoparticles were also produced via hydrothermal method and performed photocatalytic measurements through the degradation of methylene blue [34]. In an interesting study, YVO_4 powders produced by the combustion and hydrothermal method were used in RhB dye degradation and embryotoxicity tests of zebrafish and RhB solutions degraded using these powders [35].

To increase the photocatalytic activity of YVO_4, some ways can be followed such as composition engineering and doping. Cai et al. produced YVO_4/g-C_3N_4 composites and evaluated the photocatalytic activity of the composites selecting RhB as a model pollutant and these composites exhibited higher degradation efficiency than the pristine g-C_3N_4 [29]. Chen et al. studied the photocatalytic performance of hydrothermally synthesized MoS_2/YVO_4 composites in methyl orange degradation and H_2 evolution [36].

Doping is the other strategy to increase the photocatalytic ability of YVO_4 powders. For this purpose, several studies have been performed. The photocatalytic performance of hydrothermally synthesized Ag doped YVO_4 nanoparticles were investigated by the degradation of MB under visible light [37]. Doping YVO_4 with trivalent rare-earth ions is has gained great popularities in photocatalytic applications, as they show excellent properties for lasers, phosphors, or other optical applications. In an important paper, Shiraishi et al. investigated the photocatalytic activity of different amount of YVO_4: Eu^{3+} nanoparticles via degradation of methyl orange [38]. Except for photocatalysis, YVO_4 based and doped materials also find places in many technological and optical applications owing to their special 4f–5d and 4f–4f electronic transitions. Nd: YVO_4 has been used in laser crystals [39] and diode pumped solid-state lasers [40]. Eu-activated YVO_4 powders has been used as the red phosphor in color televisions and cathode ray tubes [41]. In the Shiraishi article [38] we mentioned above, they also obtained the photoluminescence (PL) spectra and proposed these nanoparticles as a model compound of a multimodal photoenergy converter. Besides the PL, the upconverting ability of lanthanide doped YVO_4 makes these materials quite remarkable recently. With upconversion nanomaterials (UCNPs), near-infrared light can be converted into visible or ultraviolet light which triggers photoreactions of photosensitive materials [42]. Lanthanide doped YVO_4 UCNPs exhibit UC emission peaks which includes f–d and f–f transitions of lanthanide ions [30, 43].

YVO_4 has been prepared with various synthesis routes in the literature such as sol–gel [44], hydrothermal [45], solvothermal [46], precipitation [47], microwave assisted [48], solution combustion [49], laser ablation [50] and solid-state reaction methods [51]. Among these techniques, solid-state reaction is one of the most common ways to obtain YVO_4 owing to its simplicity, use of open atmosphere and exhibiting higher emission intensity [52]. In this present study, undoped and La-doped YVO_4 powder samples were synthesized by a simple and efficient solid-state reaction method under an open atmosphere. Solid state reaction sintering of inorganic or ceramic powder mixtures is a way to obtain polycrystalline phosphor material from high purity solid reagents. For the reaction to occur and result in a single-phase and stable system usually a low or very high temperature is employed depending on the phase(s) targeted. The advantage of this method includes the simplicity and large-scale production of material which is synthesized in laboratory conditions [53–55]. Structural, morphological, and optical properties of the phosphors were investigated via x-ray diffraction (XRD), scanning electron microcopy (SEM), energy-dispersive X-ray (EDX) spectroscopy, photoluminescence spectrometer (PL) and UV–Vis spectrometer analyses at room temperature, respectively. It was chosen the use of lanthanum (La) as a dopant to improve reduction efficiency of La^{3+}-doped YVO_4. The photocatalytic activities of the undoped and La-doped YVO_4 powders were determined through the degradation of methylene blue (MB) dye under UV light irradiation. In the photocatalytic performances, it was observed that doping of La has an impressive effect on the photocatalytic activity of YVO_4. Also, reusability tests of the optimum photocatalyst were performed for four cycles. The possible mechanism involved in the photocatalytic reaction and photoluminescence was proposed in detail.

Experimental procedure

Materials

Yttrium (III) oxide (Y_2O_3, 99.99%, Aldrich), vanadium (V) oxide (V_2O_5, 99.5%, Stanford Materials), lanthanum (III) oxide (La_2O_3, 99.99%, Merck), and isopropyl alcohol (BioReagent, for molecular biology, ≥ 99.5%) were used as starting materials.

Further purification is not needed for these chemicals. High purity alumina crucibles were used throughout the heat treatments. The heat treatments were carried out in a muffle furnace (Nevola Reis 130/45).

Preparation of samples

Undoped and La-doped YVO_4 powder samples were prepared by typical solid-state reaction method. The stoichiometric mixtures of starting materials were precisely weighed and well mixed in zirconia bowls using zirconia balls and isopropyl alcohol in planetary mill at 250 rpm for 1 h. Then the wet mixtures were dried for 24 h at 100 °C. Two step heat treatment process was conducted at 500 °C for 4 h and at 900 °C for 4 h in open atmosphere, respectively. There was no need to grind the powders after the heat treatment. Finally, the characterization and analysis process were carried out.

Characterization

Phase purity and crystal structures were examined with a RIGAKU Rint 2000 model x-ray diffractometer, which run at 40 kV and 30 mA (Cu-Kα radiation). The particle morphology and size distributions of powders were investigated by Zeiss, SUPRA 50 VP model SEM using an accelerating voltage of 20 kV. PL spectra were recorded on two type of Fluorescence spectrophotometers which are Photon Technology International (PTI), QuantaMaster™ 30 and Hitachi F-7100. Both the PL measurement devices set with spectral slit width of 5 nm, has a Xe lamp as the excitation source and were carried out at room temperature. The optical absorption spectra properties of the samples were measured with a Shimadzu UV-1800 UV/Visible scanning spectrophotometer.

Evaluation of photocatalytic activity

Photocatalytic activities of the undoped and La-doped YVO_4 powder were evaluated by monitoring the degradation of MB under the UV light irradiation. In the experiments 6 Osram UV-C lamps with 8 watts were used as the sources of UV light. The photocatalytic activities of the powders were evaluated using a Cary 5000 UV–Visible spectrophotometer. All measurements were carried out at room temperature and aqueous MB dye solution prepared at a concentration of 5 ppm was used as the model of pollutant. After adding 50 mg of powders into the MB solution, it was first stirred for 60 min in the dark for adsorption–desorption equilibration. Then, photocatalytic activities were evaluated by absorbance measurements of 3 ml of MB dye solution collected at 15 min intervals.

Results and discussions

Structural analysis

To investigate the effect of La addition on the crystal structure of YVO_4, XRD analyses of the undoped and La-doped YVO_4 powders have been employed. Figure 1(a) and (b) show XRD diffractograms of samples prepared with solid-state reaction method. It was found that all the strong diffraction lines correspond to expected (211), (400), (433) and (600) diffraction reflections of crystalline tetragonal type crystal structure of YVO_4 (JCPDS card no: 17-0341).The XRD pattern of undoped and the La-doped YVO_4 contain same YVO_4 diffraction lines with similar relative intensities and no other diffraction lines related with any lanthanum based compounds like La_2O_3 and $La(OH)_3$, or other impurity phases were detected within the detection limit of the XRD. In the previous studies, thermal equilibrium solubility limit of La in YVO_4 was found as 6 at.% with coprecipitation method [38]. In this study, the dopant amount of YVO_4 is chosen much lower than the solubility of La in YVO_4. Therefore, according to XRD results, substitutional incorporation of the La^{3+} ions into YVO_4 crystal is expected for the studied dopant concentration.

To obtain detailed structural information, the crystallite size (D, in nm) of the powders were calculated by Scherrer's Eq. (1) using the XRD line broadening method:

$$D = 0.9\lambda/\beta\cos\theta \quad (1)$$

where λ is the X-ray wavelength for CuKα, β is the full width in radians half maximum of the diffraction line and θ is the Bragg angle of (211) peak. β is determined by $\beta = (\beta_{obs}{}^2 - \beta_{ins}{}^2)$, β_{obs} is the measured broadening and β_{ins} is the instrumental broadening caused by the diffractometer. First, a decrease is observed on crystallite size, D, with La dopant. D value of 45.5 nm and 30.9 nm were obtained for undoped and La-doped YVO_4, respectively, which suggest that there can be hindering of the

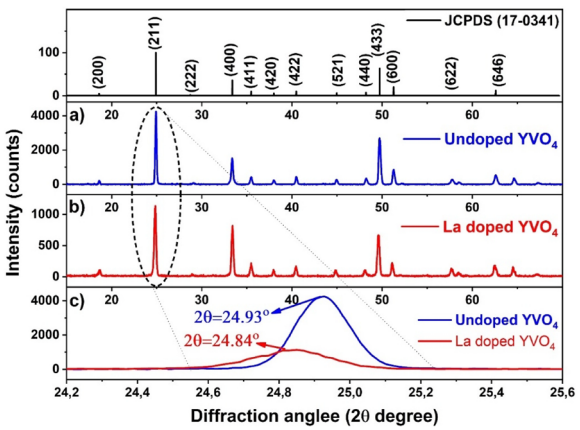

Figure 1: XRD pattern of (a) undoped and (b) La-doped YVO_4 powder. (c) The partially enlarged XRD pattern of undoped and doped powders.

crystal growth by the substitutionally incorporation of La^{3+} ions into YVO_4 crystal structure.

The effect of the La incorporation on the YVO_4 can be also investigated by examining the peak intensities and positions of YVO_4 patterns as shown [Fig. 1(c)]. It is found that the relative (211) peak intensities of undoped YVO_4 drastically decreased by La doping which implies that dopant atoms inhibit the crystal growth of YVO_4 particles at preferential growth direction. Furthermore, (211) diffraction line positions of undoped and La doped samples were determined as $2\theta = \sim 24.93°$ and $\sim 24.84°$, respectively. According to XRD spectra, insignificant peak shift is observed to relatively lower 2θ values. The lattice parameters (a) and (c) variation are also tabulated to observe doping effect. For undoped YVO_4 particles, the lattice constants (a) and (c) are calculated as 7.135 and 6.27 Å, respectively. However, YVO_4:La^{3+} powder demonstrates a slight lattice expansion with calculated lattice parameters (a) = 7.14 Å and (c) = 6.31 Å. The lattice expansion observed in the La-doped sample can be attributed to the substitution of La^{3+} ions into the Y^{3+} sites due to larger ionic radius of La^{3+} (1.172 Å) than that of Y^{3+} (1.140 Å) for the same coordination number [56]. It is normal that this expansion (hence the peak shift in the XRD pattern) has been sensitively affected as the doping rates are low. This perturbation on lattice parameters depending on La addition is preliminarily evident that incorporated La ions was selectively substitute into Y^{3+} sites of YVO_4 crystal.

Morphological and elemental analysis

The SEM photographs of the undoped and La-doped YVO_4 phosphor powders [Figs. 2(a) and 3(a)] exhibit partially agglomerated grains and irregular particles. The EDS profiles of both phosphor powders [Figs. 2(b) and 3(b)] indicate the presence of Yttrium, Vanadium, and Oxygen elements in each sample. Furthermore, in the EDS profile of La-doped YVO_4 powder, additional peaks related with lanthanum were observed.

Photoluminescence of undoped and La-doped YVO_4

The PL excitation spectra of undoped and La^{3+}-doped YVO_4 powders in Fig. 4(a) show same excitation peaks and considerable number of emission peaks between 450 and 750 nm, representing the similar positions of peaks by varying intensities. The PL emission spectrum of undoped YVO_4 has two clear

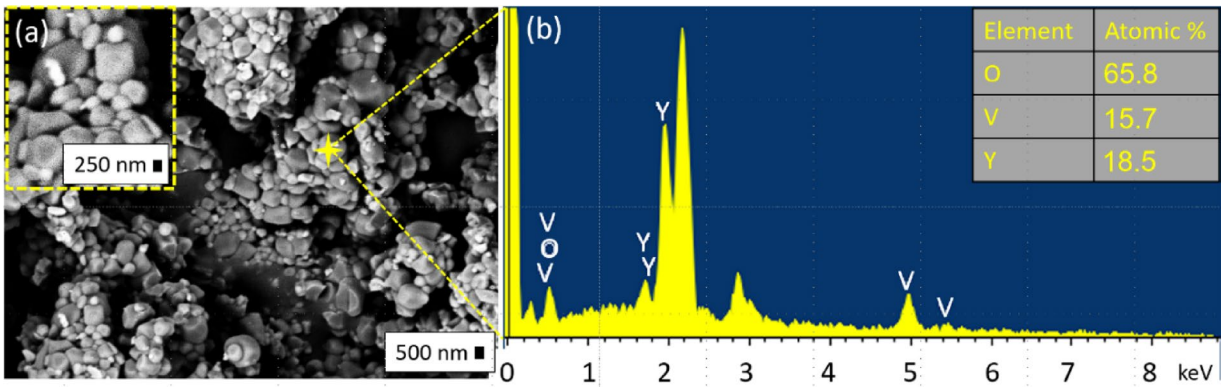

Figure 2: SEM image and EDS profile of undoped YVO_4 powder.

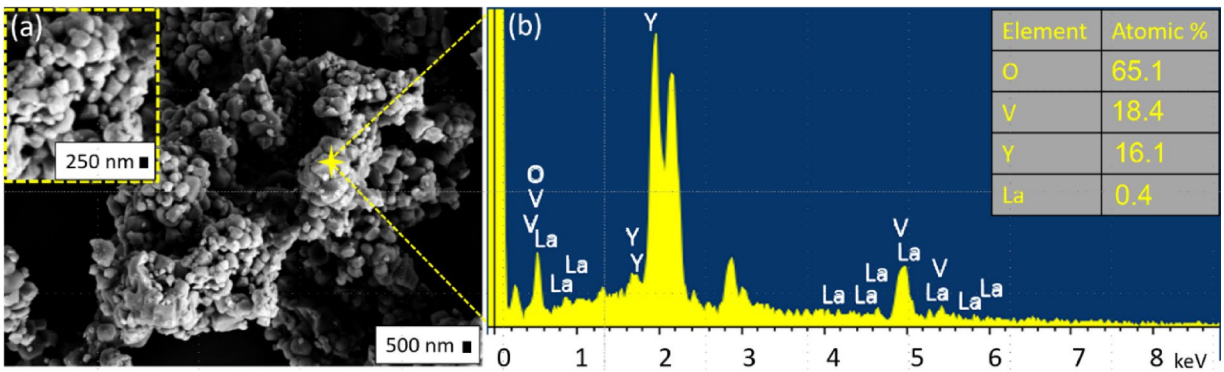

Figure 3: SEM image and EDS profile of La-doped YVO_4 powder.

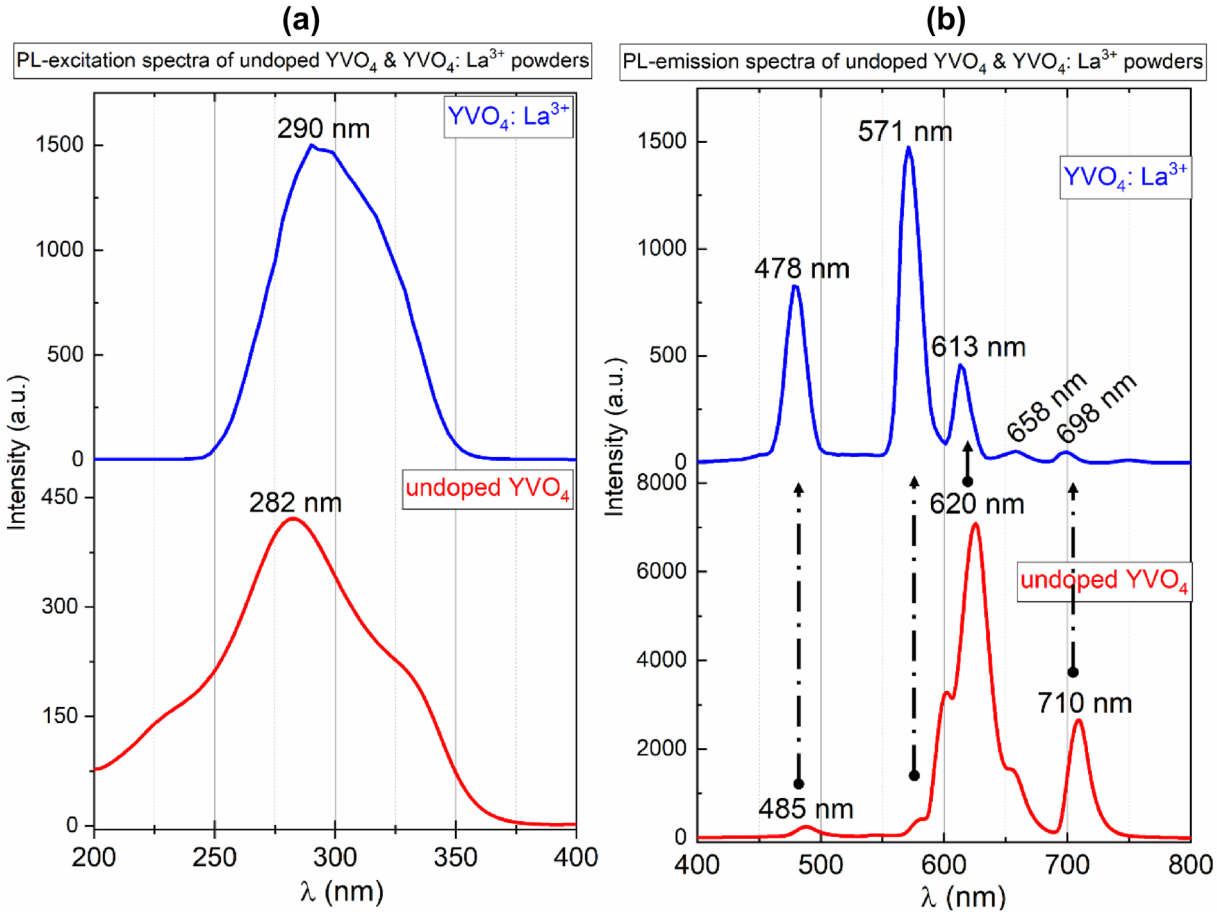

Figure 4: PL excitation and emission spectra of undoped and La-doped YVO_4 powders.

peaks in the wavelength range of 600–800 nm [Fig. 4(b)] which the major peak is at 620 nm. The other peak at 710 nm can be related to the recombination of electrons and holes at oxygen vacancies in YVO_4. The maximum intensity emission peak is located at 571 nm for La^{3+} doped YVO_4powder may be assigned to singly ionized oxygen vacancies which became dominated after La doping. With the La doping, emission bands from 450 to 650 nm were greatly suppressed and emission around 571 nm became the dominated component on the emission spectra of YVO_4: La^{3+}. The red luminescence centered at 620 nm was suppressed with respect to the blue one (at 478 nm) and the yellowish green one (at 571 nm) which are also the low intensity bands of undoped YVO_4. This indicates La doping modifies intrinsic lattice defects and intensively changes luminescence characteristic with respect to luminescence of undoped YVO_4 [57, 58].

PL excitation and emission spectra given in Fig. 4 depicts the similar luminescence characteristics of undoped and La-doped YVO_4 powder samples. The reason for red-shift from 282 to 290 nm in PL excitation spectra of undoped and La-doped YVO_4 powders, respectively can be assigned to the La doping, hence O^{2-}-La^{3+} charge transfer (CT) from oxygen 2p excited state to La^{3+} 4f state and O^{2-}-V^{5+} CT from oxygen 2p states to the empty d states of central vanadium in the VO_4^{3-} group, indicating that there is a strong energy migration from host to La^{3+} dopant ion in tetragonal YVO_4 [59].

Further, the detailed study of PL emission spectrum of undoped YVO_4 powder is shown in Fig. 5. The intense broad emission peak centered at 620 was deconvoluted using Gaussian fitting in the wavenumber (cm^{-1}) unit of energy to be able to interpret and demonstrate in detail the various defects/vacancies present in the system, as shown in Fig. 5. All these peaks combined with the major peak at 16,130 cm^{-1} (620 nm) obtained after deconvolution could be specified to emission as shallow and deep level trap states. Hence, it can be said that oxygen vacancies are the prime defects responsible for PL emission. The emission peak at 485 nm for undoped YVO_4 could correspond to characteristic intrinsic emission of VO_4^{3-} groups [60] defect related luminescence and/or surface impurities such as oxygen vacancies, intrinsic defects and surface state and intrinsic metal ions in YVO_4 crystal formed during growth. Accordingly, the effect of La^{3+} dopant ion has emerged based on the luminescence properties of the undoped material since they have same host

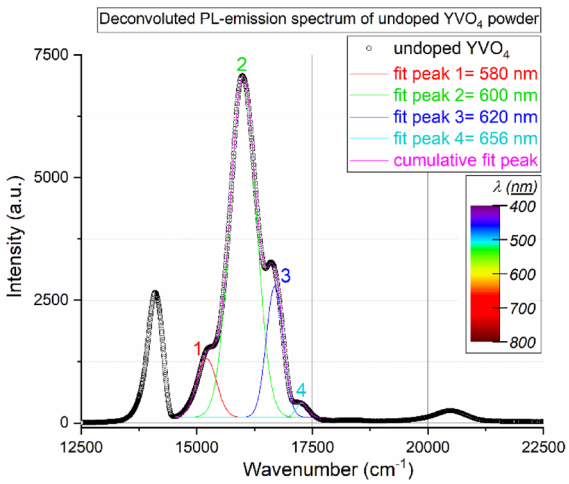

Figure 5: The deconvoluted PL emission spectrum of undoped YVO_4 powder.

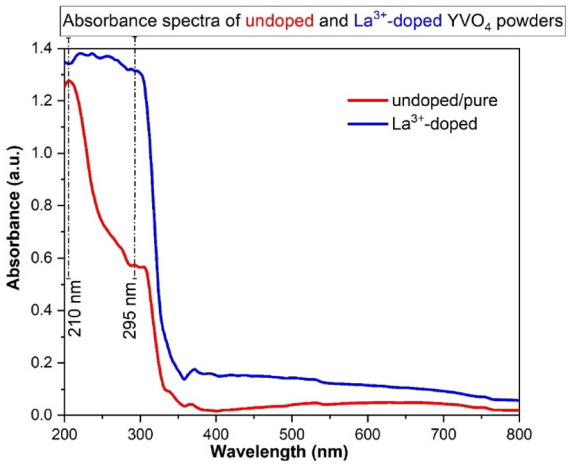

Figure 6: Absorption spectra of undoped and La-doped YVO_4 powders.

crystal. In previous studies with similar results demonstrates doping of impurities with different oxidation state can create or increase defect levels [61, 62]. The impurity ions could give raise to either radiative or non-radiative recombination. In this case and studied material, La^{3+} ion plays a significant role in modifying the defect chemistry of YVO_4 which can be clearly seen in the variation in PL intensities between undoped and La doped YVO_4. The effect of La additive on lattice is as follows: Along with doping, La^{3+} ion migrates inside the YVO_4 lattice and occupies the vacant site. There could not be charge imbalance and ionic radii mismatch affect because it was supposed to be that La^{3+} ions could substitute the Y^{3+}-sites since ionic radii are close to each other ($La^{3+} = 1.172$ Å vs $Y^{3+} = 1.140$ Å). The defects in YVO_4 may also vary with synthesis method and condition, particle size and morphology, hence, the emission peak at 485 nm, which is of relatively low intensity compared to the others is related to deep level defects of La-doped YVO_4.

Absorption spectra of undoped and La-doped YVO_4

Figure 6 shows the absorption spectra of undoped and La-doped YVO_4 powders. It can be clearly made inference that both the samples are nearly transparent in the visible region between 400 and 800 nm. Absorption spectrum of La-doped sample being a little more evident and severe, also exhibit an intense band-to-band absorption originated from the contribution of $^1A_1 \rightarrow {}^1T_1$ charge transition around 300 nm overlapped with $^1A_1 \rightarrow {}^1T_2$ charge transition at between 200 and 350 nm of VO_4^{3-} groups. Additionally, the powder colors formed in both undoped and La-doped YVO_4 samples have a light-yellow color, which can be attributed to the reduction of V^{5+} to V^{4+}, subsequently formed V^{4+} defects and oxygen vacancies. It can be concluded that the formation of V^{4+} defects is rather related with redox between Ln^{3+} (here, Ln means La) ions and different types of vanadium ions [60, 63].

Energy band gap (E_g) of the undoped and La doped YVO_4 nanoparticles were obtained using the well-known Tauc plot which is depicted in Fig. 7. Tauc method relies on the following equation:

$$(\alpha h\upsilon)^{1/n} = A(E_g - h\upsilon) \quad (2)$$

where α is the absorption coefficient, $h\upsilon$ is the energy of the incident photon, A is a constant and n depends on the optical transition of the material. YVO_4 possess a direct transition ($n = 1/2$) and a band gap of 3.8 eV [28]. As given in Fig. 7, E_g of undoped YVO_4 is obtained as 3.8 eV from fit of the red curve which is consistent with the literature. On the other hand, E_g of the La^{3+} doped YVO_4 is determined as 3.54 eV from the fit of

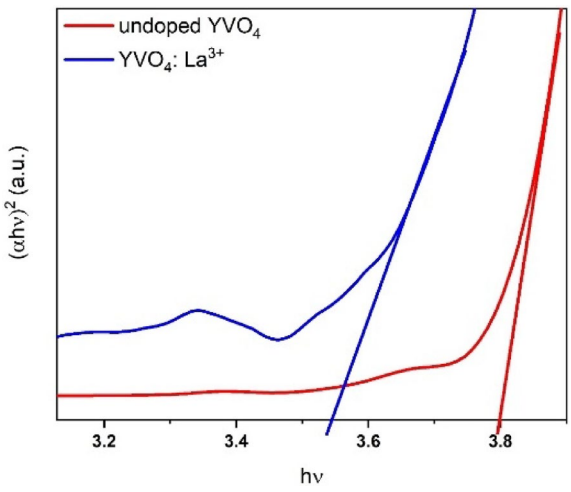

Figure 7: The Tauc plots used to calculate the band gap for undoped and La-doped YVO_4.

the blue curve. This decrease in energy band gap with doping is highly desirable for the photocatalytic performances. It is obvious that doping YVO_4 with La will provide an increase in the photocatalytic activity due to formation of new localized energy levels between valence and conduction band.

Photocatalytic activity of YVO_4 phosphors

To understand the influence of lanthanum dopant on the photoactivity of the YVO_4, the photocatalytic activities of undoped and La-doped YVO_4 powders were evaluated by degradation of MB dye under UV light irradiation. Before performing photocatalytic activity measurements, to investigate adsorption behavior of MB on the surfaces of the catalyst nanoparticles, 100 mL dye solutions without catalyst or containing nanoparticles were kept under 1-h dark conditions. Prepared solutions were then exposed to UV light at room temperature. A photocatalytic reaction was carried out with a UV light exposure time of 180 min. The wavelength of maximum absorbance of MB at 664 nm was used for the measurement of MB concentration. To investigate the effects of the catalyst dosage (0 to 50 mg in 100 mL, 5 ppm MB solution) on the removal of MB dye molecule, firstly MB solution without catalyst addition was irradiated under UV light. UV–Vis adsorption spectra of MB solution without catalyst addition is shown as inset figure in Fig. 8(a). The absorption peaks (664 nm) of the catalysis-eliminated solution remained almost unchanged (inset figure) shows the stability of the MB. The time dependent UV–Vis adsorption spectra of MB solution in the presence of 20 mg undoped YVO4 is shown in Fig. 8(a). Nearly same adsorption maxima at the initial dye solution and solution after 1 h stirring in the dark indicates that neither adsorption nor self-decomposition of MB is not observed during stirring in dark and so the amount of adsorption on YVO4 nanoparticles is neglectable.

The intensity of UV–Vis spectrum of 20 mg undoped YVO_4 added MB solution progressively decreased as the irradiation time (0–180 min) increase under the influence of light, shows that the YVO_4 catalyst degrades the stable MB molecules over time. The insensible change in the intensity of the adsorption peaks of MB solution (inset figure) suggests that electron transfer ratio from the excited MB molecules to YVO_4 nanoparticles is also negligible. Furthermore, the adsorption peaks in the presence of 20 mg catalyst YVO_4 nanoparticles show a slightly hypsochromic shift (blue shift) which can be attributed to N-demethylation of MB [64].

To determine the optimum photocatalyst dosage for achieving the maximum photocatalytic activity and the minimum cost and energy, the photocatalytic degradation process was also repeated with 35 and 50 mg undoped YVO_4 catalyst addition. Figure 8(b) exhibits the temporal profile of the photocatalytic degradation of MB solution with the addition of 20, 35 and 50 mg YVO_4 nanoparticles. Concentration change of MB molecules without catalyst addition is also given in Fig. 8(b) for comparison. It was observed that MB does not display any activation under UV light without catalyst addition, thus, all degradation observed in the dye solution containing catalyst can be addressed to catalyst effect of the YVO_4 nanoparticles. The remaining dye amount reduces over the time in all studied catalyst dosage. With the increase in the YVO_4 dosage, the increasing tendency in the dye degradation activity was observed as a function of time. This can be explained with the higher catalyst dosage promotes the higher number of photons absorbed on the catalyst surface, the higher number of generated electron/hole pairs and thus

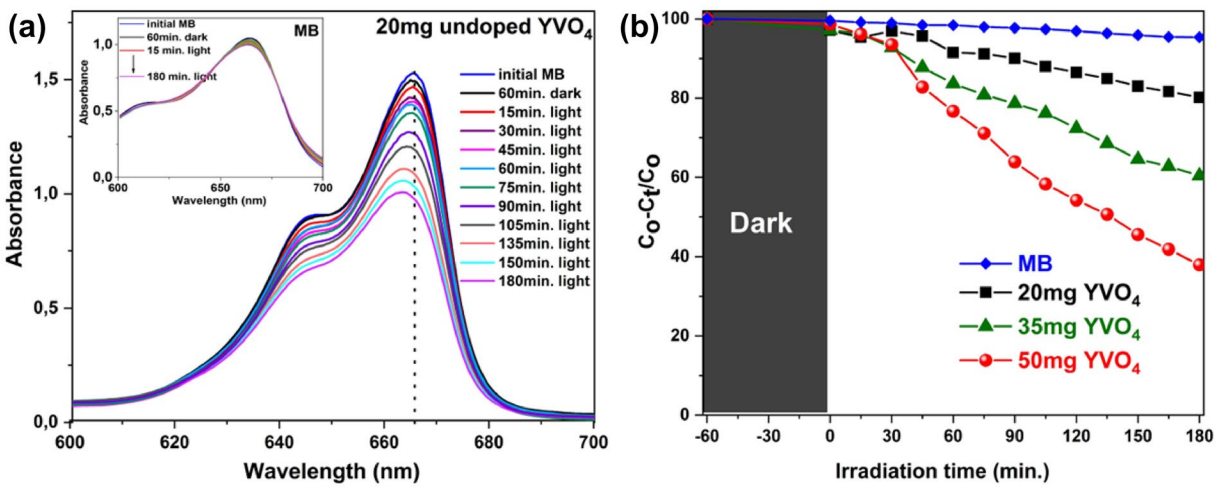

Figure 8: (a) Real-time UV–Vis absorbance spectra of the MB solution containing 20 mg undoped YVO_4 nanoparticles. (b) The photo-decomposition of MB as a function of YVO_4 dosage under UV light illumination.

a greater number of hydroxyl radicals [65]. To compare La doped sample, 50 mg of catalyst dosage with 62.1% degradation of MB was selected as the optimum catalyst dosage for further experiments.

Figure 9(a) shows the real-time absorbance spectra of MB dye solution containing 50 mg La^{3+} doped YVO_4 nanoparticles. It is clearly observed that the characteristic MB appearing at 664 nm decreases constantly with the increase of UV light irradiation time. The normalized temporal concentration changes of photocatalytic degradation of MB aqueous solution in the presence of the 50 mg YVO4 and 50 mg La^{-}doped YVO_4 photocatalysts were shown in Fig. 9(b). MB degradation behavior in the presence of P25 is also given in Fig. 9(b) for compassion purpose. As seen in Fig. 9(b), La-doped YVO_4 with 76.7% degradation efficiency led to more degradation under UV light illumination compared to the undoped one (62.1%). These results show that the photocatalytic activity of YVO_4 changes and enhances with the substitutional incorporation of La^{3+} ions into YVO_4 crystal structure. The photocatalytic degradation rate of MB dye solutions fits a pseudo-first-order reaction model which is based on the Langmuir–Hinshelwood mechanism and can be calculated from the following equation:

$$-\ln\frac{C_t}{C_0} = k_{app}t \tag{3}$$

where C_0 is the initial concentration of the dye, C_t is the concentration at irradiation time t and k_{app} is the apparent pseudo-first-order reaction rate constant. The plots of $-\ln(C_t/C_0)$ versus time t are given in Fig. 9(c) for UV exposure. The k_{app} values were calculated from the slope of these curves. According to the results obtained, the k_{app} values are 0.0555 min^{-1} and 0.0931 min^{-1} for YVO_4 and La-doped YVO_4 particles, respectively. This result shows that La doping increases the k_{app} value by 67%.

A possible mechanism can be proposed to explain the increasing in the photocatalytic activity as follows (Fig. 10): YVO_4 can only be excited by UV light ($\lambda < 367$ nm) due to its

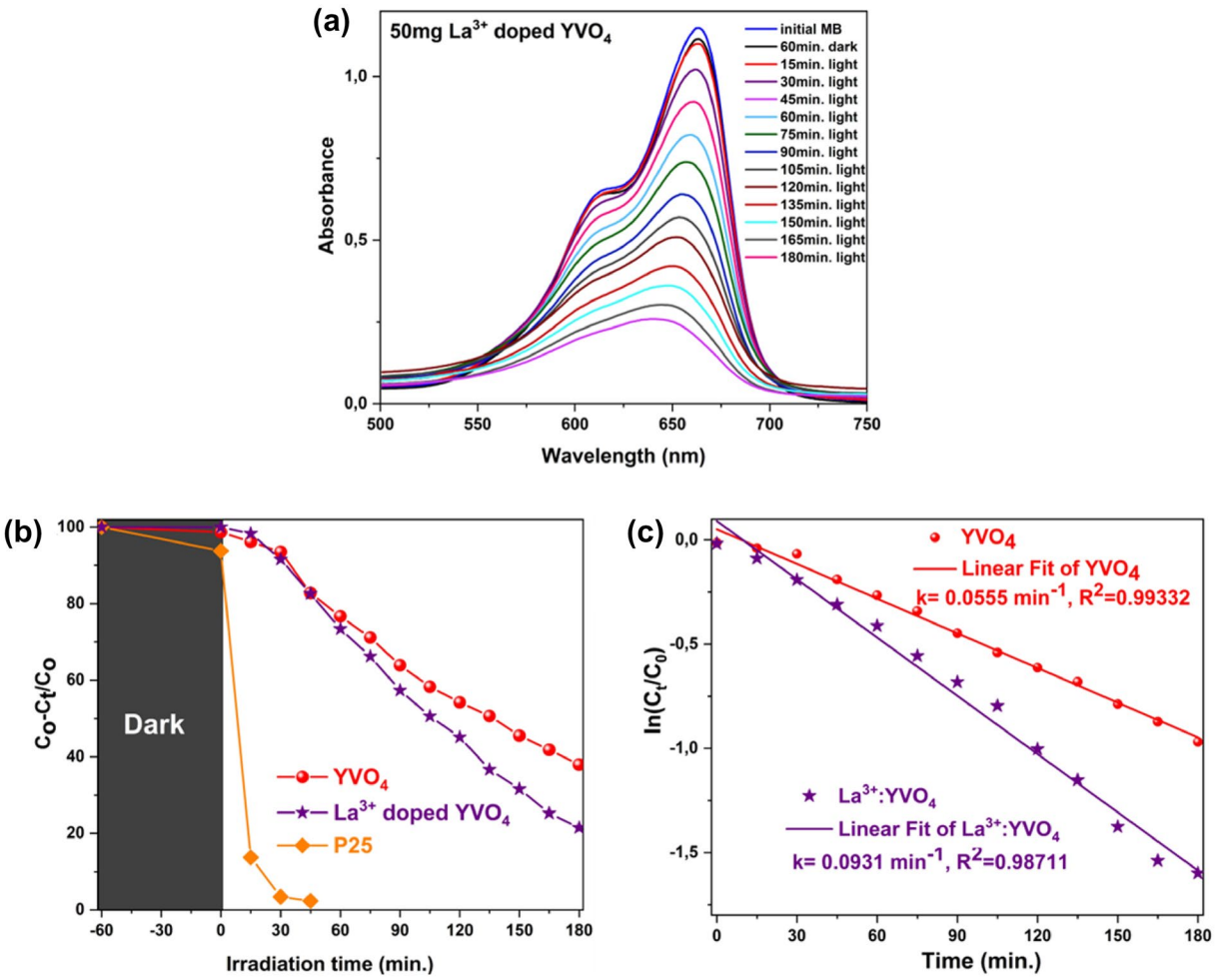

Figure 9: (a) Temporal degradations of MB aqueous solution containing 50 mg La^{3+} doped YVO_4 nanoparticles and (b) The photo-decomposition of MB as a function of 50 mg YVO_4 and La^{3+} doped YVO_4 nanoparticles under UV light illumination. The decomposition behavior of P25 is also given for comparison purposes (c) Fitted data of the pseudo first order kinetics of the undoped YVO_4 and La-doped YVO_4 powders.

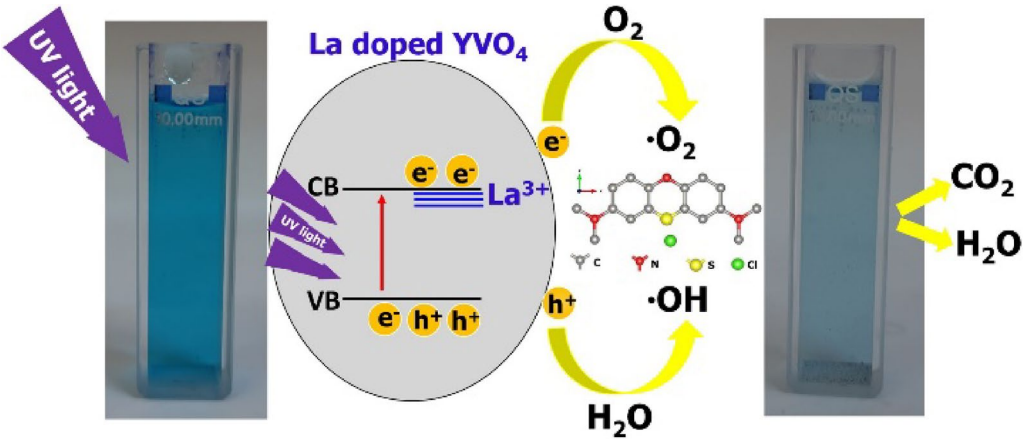

Figure 10: The representative mechanism of photocatalytic activity of La doped YVO_4.

wide band gap (3. 8 eV) [28]. La doping results in localized impurity levels between the conduction and valence bands. Thus, electrons can be excited from valence band to La doping energy level which provides the photo-generated electrons and holes with UV irradiation. While photo-generated electrons are captured by O_2 molecules to form superoxide radicals, the photo-generated holes are held by H_2O molecules to form hydroxyl radicals. Also, La^{3+} ions act as electron traps and decrease the electron–hole recombination rate. These trapping prevent electron and hole recombination as they migrate to the catalyst surface [66]. The recombination of electrons and holes excites the 4f electrons of the La, converting the energy corresponding to the 4f → 4f transitions into red emission [38].

In the dye removal purification processes through photocatalytic reactions, a valuable feature of the photocatalyst is their chemical stability during their reutilization since the high number of recyclability reduces the cost of the photocatalytic applications. Chemical stability is an important issue for the application. To verify the chemical stability of La-doped YVO_4 nanoparticles, the change in the relative degradation percentage of MB with recycle test were tested using 50 mg of the catalysts under the same condition with the four run experiments. After each run, all the catalysts were centrifuged, dried at 100 °C for 3 h and added to fresh dye solution to utilize for the next running test. According to Fig. 11, the catalytic performance of the La-doped YVO_4 nanoparticles displayed a slight deterioration at 3rd cycle. Herein, MB degradation amount of La-doped YVO_4 nanoparticles were determined as 78.6% (1 st run), 77.6% (2nd run), 73.1% (3rd run) and 50.9% (4th run). These results show that the photostability of La-doped YVO_4 nanoparticles diminished slowly with 3rd time reused. Therefore, the proposed photocatalyst

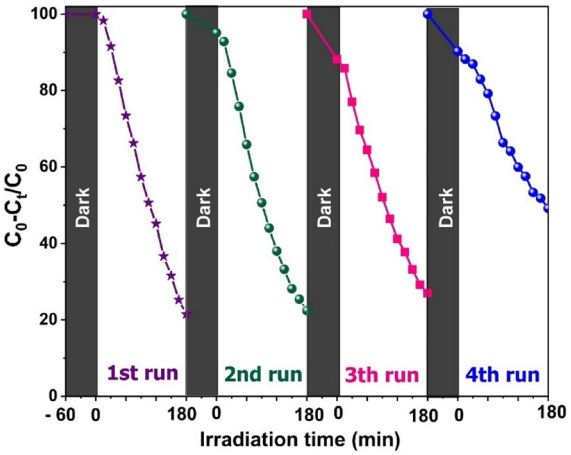

Figure 11: Stability performance of La-doped YVO_4 nanoparticles for MB degradation under simulated UV light irradiation (after 60 min stirring in dark, 180 min for each cycle).

can be utilized for continuous treatment of industrial water purification process.

Conclusion

Yttrium vanadate-based powder samples were successfully prepared with solid-state reaction method at low sintering temperatures under an open atmosphere. Both the undoped and La-doped samples show the tetragonal YVO_4 phase. The effect of the La doping was also confirmed by the characterizations. Due to bigger ionic radius of La^{3+} ($r_{La}{}^{3+} = 1.172$ Å) than that of the Y^{3+} ($r_Y{}^{3+} = 1.401$ Å), the positional shift in the XRD peaks, the change in the peak intensity and broadening of the diffraction peaks suggest that the substitutional incorporation of La^{3+} ions into Y^{3+} sites of the YVO4 crystal structure. Powder samples both exhibit partially agglomerated particles with irregular

shape and size. The EDS profile of both powders also represents the presence of all elements what in each sample must have. The PL studies demonstrate the characteristic emission peaks of undoped YVO_4 have not changed prominently after the introduction of La^{3+} ions while the luminescence intensity varied. The PL emission spectrum of pure YVO_4 has two clear peaks located at 620 and 710 nm in the wavelength range of 600–800 nm which can be related to shallow and deep level trap states and the recombination of electrons and holes at oxygen vacancies in YVO_4, respectively. The major emission peak (at 571 nm) of La^{3+} doped YVO_4: nanoparticles may be assigned to singly ionized oxygen vacancies which became dominated after La doping. Moreover, emission bands between 450 and 650 nm were significantly suppressed in YVO_4: La^{3+}. Therefore, La doping may modify the intrinsic lattice defects and effectively changes luminescence characteristic with respect to PL characteristics of undoped YVO_4. The effect of La doping on the YVO_4 can also be seen from the absorption spectra. With the La doping, there exists an intense band-to-band absorption originated from the contribution of $^1A_1 \rightarrow {}^1T_1$ charge transition around 300 nm overlapped with $^1A_1 \rightarrow {}^1T_2$ charge transition at between 200 and 350 nm of VO_4^{3-} groups. In addition, the energy band gap of the La-doped YVO_4 was measured as 3.5 eV which is the sign of the improved photocatalytic performance of the doped YVO_4. The improvement in the photocatalytic performance of the doped powders can be attributed to localized energy levels, trapping of the electrons by La^{3+} ions and energy conversion of the 4f electrons of lanthanum. According to the results, La-doped YVO_4 is an effective photocatalyst for water treatment.

Author contributions

EK performed the sample preparation and experimental works. All the authors carried out the analysis, manuscript writing, and did final editing.

Funding

Not applicable

Data availability

Not applicable

Declarations

Competing interests The authors declare that they have no financial interests or personal relationships that could affect the work.

Ethical approval

The authors confirm that the present work is unpublished and not under consideration for publication elsewhere.

References

1. S.L. Postel, G.C. Daily, P.R. Ehrlich, Human appropriation of renewable fresh water. Science **271**, 785–788 (1996)
2. C.Y. Teh, P.M. Budiman, K.P.Y. Shak, T.Y. Wu, Recent advancement of coagulation-flocculation and its application in wastewater treatment. Ind. Eng. Chem. Res. **55**, 4363–4389 (2016)
3. H. Selcuk, Decolorization and detoxification of textile wastewater by ozonation and coagulation processes. Dyes Pigm. **64**, 217–222 (2005)
4. M.A. Al-Nuaim, A.A. Alwasiti, Z.Y. Shnain, The photocatalytic process in the treatment of polluted water. Chem. Pap. **77**, 677–701 (2023)
5. S.N. Ahmed, W. Haider, Heterogeneous photocatalysis and its potential applications in water and wastewater treatment: a review. Nanotechnology **29**, 342001 (2018)
6. S. Li, M. Cai, C. Wang et al., Ta_3N_5/CdS core-shell s-scheme heterojunction nanofibers for efficient photocatalytic removal of antibiotic tetracycline and cr(VI): performance and mechanism insights. Adv. Fiber Mater. **5**, 994–1007 (2023). https://doi.org/10.1007/s42765-022-00253-5
7. S. Li, J. Chen, S. Hu, H. Wang, W. Jiang, X. Chen, Facile construction of novel Bi2WO6/Ta3N5 Z-scheme heterojunction nanofibers for efficient degradation of harmful pharmaceutical pollutants. Chem. Eng. J. **402**, 126165 (2020)
8. A. Saravanan, P.S. Kumar, D.-V.N. Vo, P.R. Yaashikaa, S. Karishma, S. Jeevanantham, B. Gayathri, V.D. Bharathi, Photocatalysis for removal of environmental pollutants and fuel production: a review. Environ. Chem. Lett. **19**, 441–463 (2021)
9. S. Li, M. Cai, Y. Liu, C. Wang, R. Yan, X. Chen, Constructing Cd0.5Zn0.5S/Bi2WO6 S-scheme heterojunction for boosted photocatalytic antibiotic oxidation and Cr(VI) reduction. Adv. Powder Mater. **2**, 100073 (2023)
10. M. Cai, C. Wang, Y. Liu, R. Yan, S. Li, Boosted photocatalytic antibiotic degradation performance of Cd0.5Zn0.5S/carbon dots/Bi2WO6 S-scheme heterojunction with carbon dots as the electron bridge. Sep. Purif. Technol. **300**, 121892 (2022)
11. A. Fujishima, K. Honda, Electrochemical photolysis of water at a semiconductor electrode. Nature **238**, 37–38 (1972)
12. Q. Guo, C. Zhou, Z. Ma, X. Yang, Fundamentals of TiO2 photocatalysis: concepts mechanisms, and challenges. Adv. Mater. **31**, 1901997 (2019)
13. K.M. Lee, C.W. Lai, K.S. Ngai, J.C. Juan, Recent developments of zinc oxide based photocatalyst in water treatment technology: a review. Water Res. **88**, 428–448 (2016)

14. L. Cheng, Q. Xiang, Y. Liao, H. Zhang, CdS-based photocatalysts. Energy Environ. Sci. **11**, 1362–1391 (2018)
15. C.B. Ong, L.Y. Ng, A.W. Mohammad, A review of ZnO nanoparticles as solar photocatalysts: synthesis, mechanisms and applications. Renew. Sustain. Energy Rev. **81**, 536–551 (2018)
16. Y. Liu, H. Yu, S. Zhan, Y. Li, Z. Lv, X. Yang, Y. Yu, Fast degradation of methylene blue with electrospun hierarchical α-Fe2O3 nanostructured fibers. J. Sol-Gel Sci. Technol. **58**, 716–723 (2011)
17. E. Keles, M. Yildirim, T. Öztürk, O.A. Yildirim, Hydrothermally synthesized UV light active zinc stannate:tin oxide (ZTO:SnO2) nanocomposite photocatalysts for photocatalytic applications. Mater. Sci. Semicond. Process. **110**, 104959 (2020)
18. S. Li, C. Wang, Y. Liu, Y. Liu, M. Cai, W. Zhao, X. Duan, S-scheme MIL-101(Fe) octahedrons modified Bi2WO6 microspheres for photocatalytic decontamination of Cr(VI) and tetracycline hydrochloride: synergistic insights, reaction pathways, and toxicity analysis. Chem. Eng. J. **455**, 140943 (2023)
19. K. Onozuka, Y. Kawakami, H. Imai, T. Yokoi, T. Tatsumi, J.N. Kondo, Perovskite-type La2Ti2O7 mesoporous photocatalyst. J. Solid State Chem. **192**, 87–92 (2012)
20 M. Cai, Y. Liu, C. Wang, W. Lin, S. Li, Novel Cd0.5Zn0.5S/Bi2MoO6 S-scheme heterojunction for boosting the photodegradation of antibiotic enrofloxacin: degradation pathway, mechanism and toxicity assessment. Sep. Purif. Technol. **304**, 122401 (2023)
21. M. Cai, Y. Liu, K. Dong, C. Wang, S. Li, A novel S-scheme heterojunction of Cd0.5Zn0.5S/BiOCl with oxygen defects for antibiotic norfloxacin photodegradation: Performance, mechanism, and intermediates toxicity evaluation. J. Colloid Interface Sci. **629**, 276–286 (2023)
22. E. Ersöz, O. AltintasYildirim, Green synthesis and characterization of Ag-doped ZnO nanofibers for photodegradation of MB, RhB and MO dye molecules. J. Korean Ceram. Soc. **59**, 655–670 (2022)
23 H. Chakhtouna, H. Benzeid, N. Zari, A. Qaiss, R. Bouhfid, Recent progress on Ag/TiO2 photocatalysts: photocatalytic and bactericidal behaviors. Environ. Sci. Pollut. Res. **28**, 44638–44666 (2021)
24. C. Wang, R. Yan, M. Cai, Y. Liu, S. Li, A novel organic/inorganic S-scheme heterostructure of TCPP/Bi12O17Cl2 for boosting photodegradation of tetracycline hydrochloride: kinetic, degradation mechanism, and toxic assessment. Appl. Surf. Sci. **610**, 155346 (2023)
25. S. Li, M. Cai, Y. Liu, C. Wang, K. Lv, X. Chen, S-Scheme photocatalyst TaON/Bi2WO6 nanofibers with oxygen vacancies for efficient abatement of antibiotics and Cr(VI): Intermediate eco-toxicity analysis and mechanistic insights. Chin. J. Catal. **43**, 2652–2664 (2022)
26. L. Hao, H. Huang, Y. Zhang, T. Ma, Oxygen vacant semiconductor photocatalysts. Adv. Func. Mater. **31**, 2100919 (2021)
27. L. Yang, G. Li, W. Hu, M. Zhao, L. Sun, J. Zheng, T. Yan, L. Li, Control over the crystallinity and defect chemistry of YVO4 nanocrystals for optimum photocatalytic property. Eur. J. Inorg. Chem. **2011**, 2211–2220 (2011)
28. M.R. Dolgos, A.M. Paraskos, M.W. Stoltzfus, S.C. Yarnell, P.M. Woodward, The electronic structures of vanadate salts: cation substitution as a tool for band gap manipulation. J. Solid State Chem. **182**, 1964–1971 (2009)
29. J. Cai, Y. He, X. Wang, L. Zhang, L. Dong, H. Lin, L. Zhao, X. Yi, W. Weng, H. Wan, Photodegradation of RhB over YVO4/g-C3N4 composites under visible light irradiation. RSC Adv. **3**, 20862–20868 (2013)
30. Y.K. Kshetri, C. Regmi, H.-S. Kim, S.W. Lee, T.-H. Kim, Microwave hydrothermal synthesis and upconversion properties of Yb3+/Er3+ doped YVO4 nanoparticles. Nanotechnology **29**, 204004 (2018)
31. W. Ryba-Romanowski, YVO4 crystals - puzzles and challenges. Cryst Res Technol **38**, 225–236 (2003)
32. H. Xu, H. Wang, H. Yan, Preparation and photocatalytic properties of YVO4 nanopowders. J. Hazard. Mater. **144**, 82–85 (2007)
33. Y. Liu, J. Ma, C. Dai, Z. Song, Y. Sun, J. Fang, C. Gao, J. Zhao, Low-temperature synthesis of YVO4 nanoparticles and their photocatalytic activity. J. Am. Ceram. Soc. **92**, 2791–2794 (2009)
34. R.M. Mohamed, F.A. Harraz, I.A. Mkhalid, Hydrothermal synthesis of size-controllable Yttrium Orthovanadate (YVO4) nanoparticles and its application in photocatalytic degradation of direct blue dye. J. Alloy. Compd. **532**, 55–60 (2012)
35. C.M. Aiube, T.M. Lobo, D. Sousa-Moura, I.B.M. Ferraz, M.E. Osugi, C.K. Grisolia, R. Oliveira, I.T. Weber, Study of YVO4 as a photocatalyst: Correlation between synthetic route and ecotoxicity. J. Environ. Chem. Eng. **6**, 2846–2854 (2018)
36. Q. Chen, C. Zhao, Y. Wang, Y. Chen, Y. Ma, Z. Chen, J. Yu, Y. Wu, Y. He, Synthesis of MoS2/YVO4 composite and its high photocatalytic performance in methyl orange degradation and H2 evolution. Sol. Energy **171**, 426–434 (2018)
37. R.M. Mohamed, E.S. Aazam, Novel Ag/YVO4 nanoparticles prepared by a hydrothermal method for photocatalytic degradation of methylene-blue dye. J. Ind. Eng. Chem. **20**, 4377–4381 (2014)
38. Y. Shiraishi, S. Takeshita, T. Isobe, Two photoenergy conversion modes of YVO4:Eu3+ nanoparticles: photoluminescence and photocatalytic activity. J. Phys. Chem. C **119**, 13502–13508 (2015)
39. H.J. Zhang, L. Zhu, X.L. Meng, Z.H. Yang, C.Q. Wang, W.T. Yu, Y.T. Chow, M.K. Lu, Thermal and laser properties of Nd:YVO4 crystal. Cryst. Res. Technol. **34**, 1011–1016 (1999)
40. R.A. Fields, M. Birnbaum, C.L. Fincher, Highly efficient Nd:YVO4 diode-laser end-pumped laser. Appl. Phys. Lett. **51**, 1885–1886 (1987)

41. A.K. Levine, F.C. Palilla, A new, highly efficient red-emitting cathodoluminescent phosphor (YVO4:Eu) for color television. Appl. Phys. Lett. **5**, 118–120 (1964)
42. S. Wu, H.-J. Butt, Near-infrared-sensitive materials based on upconverting nanoparticles. Adv. Mater. **28**, 1208–1226 (2016)
43. T. Chen, K. Li, H. Mao, Y. Chen, J. Wang, Preparation and upconversion emission investigation of the YVO4: Yb3+/Tb3+/Eu3+ nanomaterials and their coupling with the Au nanoparticles. Cryst. Res. Technol. **55**, 2000001 (2020)
44. E.V. Golyeva, D.V. Tolstikova, I.E. Kolesnikov, M.D. Mikhailov, Effect of synthesis conditions and surrounding medium on luminescence properties of YVO4:Eu3+ nanopowders. J. Rare Earths **33**, 129–134 (2015)
45. H. Zhu, X. Li, Y. Liu, J. Chen, L. Gao, J. Chen, W. Lin, Y. Li, H. Chi, Hydrothermal synthesis of YVO4:Eu3+ micron-sized spheres and their photoluminescence properties. Mater. Res. Express **6**, 086218 (2019)
46. G. Jia, Y. Song, M. Yang, Y. Huang, L. Zhang, H. You, Uniform YVO4:Ln3+ (Ln=Eu, Dy, and Sm) nanocrystals: solvothermal synthesis and luminescence properties. Opt. Mater. **31**, 1032–1037 (2009)
47. K. Vignesh, A. Suganthi, B.-K. Min, M. Rajarajan, M. Kang, Designing of YVO4 supported β-AgI nano-photocatalyst with improved stability. RSC Adv. **5**, 576–585 (2015)
48. L. Shirmane, C. Feldmann, V. Pankratov, Comparing the luminescence processes of YVO4: Eu and core-shell YVO4@YF3 nanocrystals with bulk-YVO4:Eu. Physica B **504**, 80–85 (2017)
49 R. Gangadharachar, G.T. Chandrappa, Solution combustion synthesis of YVO4 nanopowder using V2O5.nH2O Gel: photodegradation studies. Trans. Indian Ceram. Soc. **80**, 47–54 (2021)
50. H. Wang, O. Odawara, H. Wada, Facile and chemically pure preparation of YVO4:Eu3+ colloid with novel nanostructure via laser ablation in water. Sci. Rep. **6**, 20507 (2016)
51. V. Natarajan, A.R. Dhobale, C.-H. Lu, Preparation and characterization of tunable YVO4: Bi3+, Sm3+ phosphors. J. Lumin. **129**, 290–293 (2009)
52. P. Kumari, P.K. Baitha, J. Manam, Structural and photoluminescence properties of red-light emitting YVO4:Eu3+ phosphor synthesized by combustion and solid-state reaction techniques: a comparative study. Indian J. Phys. **89**, 1297–1306 (2015)
53. I.P. Sahu, D.P. Bisen, R.K. Tamrakar, K.V.R. Murthy, M. Mohapatra, Studies on the luminescence properties of CaZrO3:Eu3+ phosphors prepared by the solid state reaction method. J. Sci.: Adv. Mater. Devices **2**, 69–78 (2017)
54. D. Kim, H.E. Kim, C.H. Kim, Enhancement of long-persistent phosphorescence by solid-state reaction and mixing of spectrally different phosphors. ACS Omega **5**, 10909–10918 (2020)
55. E. Karacaoglu, E. Ozturk, M. Uyaner, M.D. Losego, Atomic layer deposition (ALD) of nanoscale coatings on SrAl2O4-based phosphor powders to prevent aqueous degradation. J. Am. Ceram. Soc. **103**, 3706–3715 (2020)
56. R. Shannon, Revised effective ionic radii and systematic studies of interatomic distances in halides and chalcogenides. Acta Crystallogr. A **32**, 751–767 (1976)
57 M. Duhan, S. Bharadwaj, A. Gupta, H. Kaur, Influence of La doping on structural, photo-luminescence and magnetic properties of SnO2 nanostructures co-doped with Gdk. Mater. Lett. **302**, 130402 (2021)
58. Y.L. Huang, W.L. Zhu, X.Q. Feng, Z.Y. Man, The effects of La3+ doping on luminescence properties of PbWO4 single crystal. J. Solid State Chem. **172**, 188–193 (2003)
59. Y.X. Liu, G.X. Liu, J.X. Wang, X.T. Dong, W.S. Yu, Red-dish-orange-emitting and paramagnetic properties of GdVO4:Sm3+/Eu3+ multifunctional nanomaterials. New J. Chem. **39**, 9028–9028 (2015)
60. L.S. Yang, S.Y. Peng, M.L. Zhao, L.S. Yu, New synthetic strategies for luminescent YVO4:Ln(3+) (Ln = Pr, Sm, Eu, Tb, Dy, Ho, Er) with mesoporous cell-like nanostructure. Opt. Mater. Express **8**, 3805–3819 (2018)
61. Y.F. Wang, J. Su, Z.H. Lin, J.C. Zhang, J.J. Chang, Y. Hao, Recent progress on the effects of impurities and defects on the properties of Ga2O3. J. Mater. Chem. C **10**, 13395–13436 (2022)
62. T. Tsuzuki, R.L. He, A. Dodd, M. Saunders, Challenges in determining the location of dopants, to study the influence of metal doping on the photocatalytic activities of ZnO nanopowders. Nanomaterials-Basel **9**, 481 (2019)
63. Z.Y. Hou, P.P. Yang, C.X. Li, L.L. Wang, H.Z. Lian, Z.W. Quan, J. Lin, Preparation and luminescence properties of YVO4: Ln and Y(V, P)O-4: Ln (Ln = Eu3+, Sm3+, Dy3+) nanofibers and microbelts by sol-gel/electrospinning process. Chem. Mater. **20**, 6686–6696 (2008)
64. T. Zhang, T. Oyama, A. Aoshima, H. Hidaka, J. Zhao, N. Serpone, Photooxidative N-demethylation of methylene blue in aqueous TiO2 dispersions under UV irradiation. J. Photochem. Photobiol., A **140**, 163–172 (2001)
65. E. Baylan, O.A. Yildirim, Highly efficient photocatalytic activity of stable manganese-doped zinc oxide (Mn:ZnO) nanofibers via electrospinning method. Mater. Sci. Semicond. Process. **103**, 104621 (2019)
66 J.B. Kisała, G. Hörner, A. Barylyak, D. Pogocki, Y. Bobitski, Photocatalytic degradation of 4,4'-isopropylidenebis(2,6-dibromophenol) on sulfur-doped nano TiO(2). Materials (Basel) **15**, 361 (2022)